Molecular Complexity in Prestellar Cores: L183 *VS* L1544 at 3mm.

Valerio Lattanzi

CAS@MPE
Garching (Germany)

June 21, 2018

Background

- Pre-stellar cores are the first phase of the star formation:
  - chemistry and physics away from complexity arising from the proto-stellar feedback
  - exhibit complex molecular inventory and distribution
  - starless cores on the verge of star formation

Phase & Object	Age (yr)	Radius (AU)	Temp. (K)	Density (cm^{-3})	Chemical processes
1 - Pre-stellar core	$\sim 10^5$	$\sim 10^4$	7–15	10^4–10^6	Ice formation & molecular deuteration
2 - Protostellar envelope:	10^4–10^5	$\sim 10^4$			
Cold envelope		100–10^4	≤ 100	10^5–10^7	Ice formation & molecular deuteration
Hot corinos		≤ 100	≥ 100	$\geq 10^7$	Complex molecules formation
3 - Protoplanetary disk:	$\sim 10^6$	~ 200			
Outer midplane		20–200	100–10	10^8–10^6	Ice formation & molecular deuteration
Inner midplane		≤ 20	≥ 100	$\geq 10^8$	Complex molecules formation

Caselli & Ceccarelli, A&ARv 2012

Observational details

- Single-pointing observations with IRAM 30m (May 2015)
- $\alpha_{2000} = 15^h54^m08^s.6$, $\delta_{2000} = -02°52'10''.0$
- EMIR receiver (E090) at 3mm
- FTS backend: 49 kHz/channel
  7.2 GHz instantaneous bandwidth
- Frequency switching
- T_{sys} around 80–120 K
- *rms* $\sim$ 2–10 mK
- 46 molecular species

L183 at 3mm: looking for...

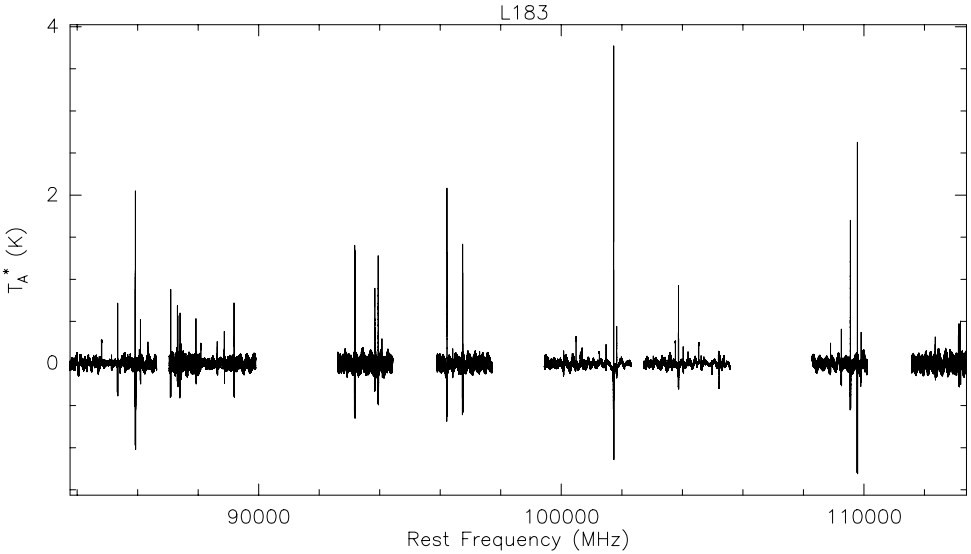

Astronomy & Astrophysics manuscript no. nco
April 17, 2018
©ESO 2018

arXiv:1804.05652v1 [astro-ph.GA] 16 Apr 2018

Letter to the Editor

Discovery of the elusive radical NCO and confirmation of H_2NCO^+ in space ⋆

N. Marcelino[1], M. Agúndez[1], J. Cernicharo[1], E. Roueff[2], and M. Tafalla[3]

[1] Instituto de Física Fundamental, CSIC, C/ Serrano 123, 28006 Madrid, Spain
[2] Sorbonne Université, Observatoire de Paris, Université PSL, CNRS, LERMA, F-92190, Meudon, France
[3] Observatorio Astronómico Nacional (OAN), C/ Alfonso XII 3, 28014 Madrid, Spain

Received ; accepted

ABSTRACT

The isocyanate radical (NCO) is the simplest molecule containing the backbone of the peptide bond, C(=O)-N. This bond has a prebiotic interest since is the one linking two amino acids to form large chains of proteins. It is also present in some organic molecules observed in space such as HNCO, NH_2CHO and CH_3NCO. In this letter we report the first detection in space of NCO towards the dense core L483. We also report the identification of the ion H_2NCO^+, definitively confirming its presence in space, and observations of HNCO, HOCN, and HCNO in the same source. For NCO, we derive a column density of 2.2×10^{12} cm^{-2}, which means that it is only ∼5 times less abundant than HNCO. We find that H_2NCO^+, HOCN and HCNO have abundances relative to HNCO of 1/400, 1/80, and 1/160, respectively. Both NCO and H_2NCO^+ are involved in the production of HNCO and several of its isomers. We have updated our previous chemical models involving NCO and the production of the CHNO isomers. Taking into account the uncertainties in the model, the observed abundances are reproduced relatively well. Indeed, the detection of NCO and H_2NCO^+ in L483 supports the chemical pathways to the formation of the detected CHNO isomers. Sensitive observations of NCO in sources where other molecules containing the C(=O)-N subunit have been detected could help in elucidating its role in prebiotic chemistry in space.

Key words. Astrochemistry – ISM: clouds, L483 – ISM: abundances – Stars: formation, low-mass Line: identification

Detected Species

Number of Atoms					
2	3	4	5	6	8
$C^{17}O$	C_2H	C_3O	c-C_3H_2	CH_3CHO	CH_3OCHO
$C^{18}O$	HCN	$HOCO^+$	l-C_3H_2	CH_3CCH	
$^{13}C^{18}O$	$HC^{15}N$	HDCS	c-$CC^{13}CH_2$		
CN	$H^{13}CN$	H_2CS	c-C_3HD		
^{13}CN	$H^{15}NC$	$H_2C^{34}S$	C_4H		
SO	$HN^{13}C$	D_2CS	t-HCOOH		
$S^{18}O$	HCO^+	HNCO	H_2CCO		
$C^{34}S$	$HC^{18}O^+$	HOCN	CH_3OH		
NS^+	HCS^+	DNCO	CH_2DOH		
	N_2H^+	NH_2D	HC_3N		
	SO_2		DC_3N		
	$^{34}SO_2$				
	OCS				

Detected Species

Number of Atoms					
2	3	4	5	6	8
$C^{17}O$	C_2H	C_3O	c-C_3H_2	CH_3CHO	CH_3OCHO
$C^{18}O$	HCN	$HOCO^+$	l-C_3H_2	CH_3CCH	
$^{13}C^{18}O$	$HC^{15}N$	HDCS	c-$CC^{13}CH_2$		
CN	$H^{13}CN$	H_2CS	c-C_3HD		
^{13}CN	$H^{15}NC$	$H_2C^{34}S$	C_4H		
SO	$HN^{13}C$	D_2CS	t-HCOOH		
$S^{18}O$	HCO^+	HNCO	H_2CCO		
$C^{34}S$	$HC^{18}O^+$	HOCN	CH_3OH		
NS^+	HCS^+	DNCO	CH_2DOH		
	N_2H^+	NH_2D	HC_3N		
	SO_2		DC_3N		
	$^{34}SO_2$				
	OCS				

Analysis

- Performed with GILDAS/CLASS and CASSIS
- Assuming LTE conditions
- Line opacity checked for each transition
  - $\tau = -ln\left[1 - \frac{T_{MB}}{f[J_\nu(T_{ex}) - J_\nu(T_{bg})]}\right]$

- Started with iCOMs (LAMs, COMs...)
- More refined analysis for CH_3OH

COMs Spectra

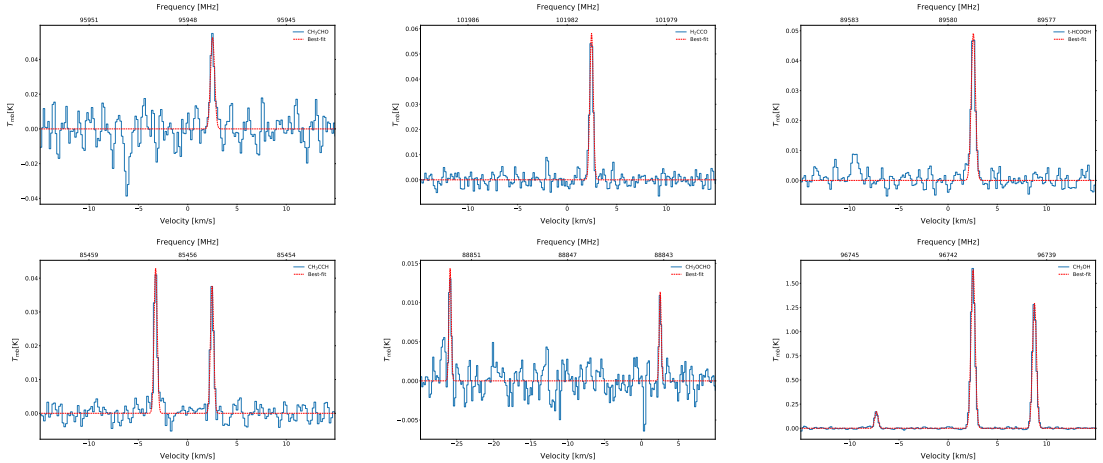

Methanol in LTE

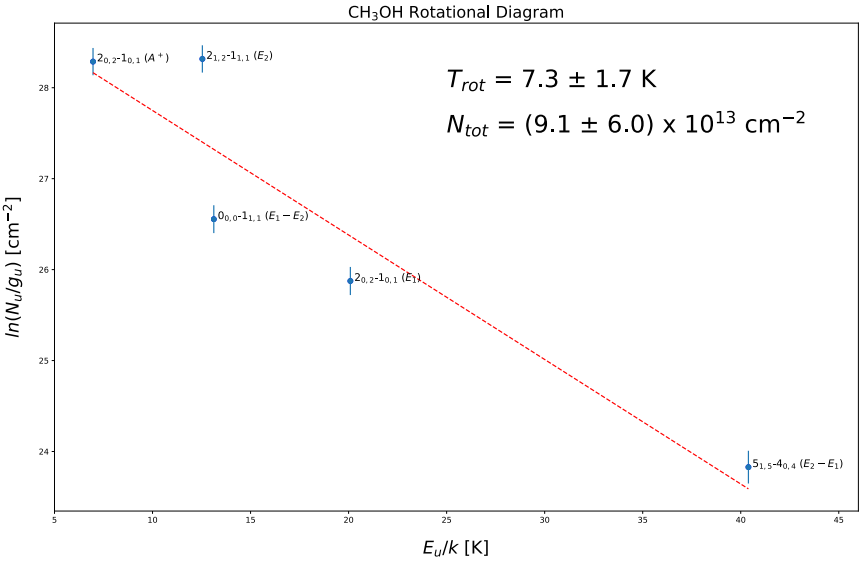

Methanol in LTE

L183

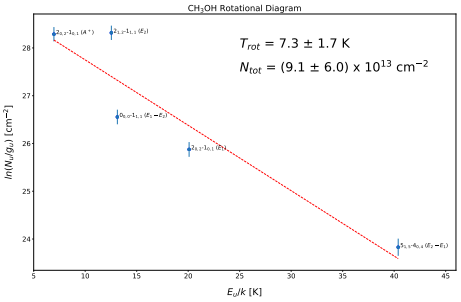

L1544

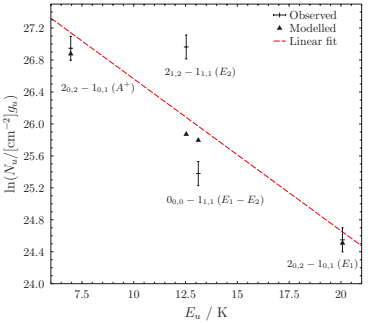

Bizzocchi +, A&A 2014

Methanol non-LTE analysis – long story short

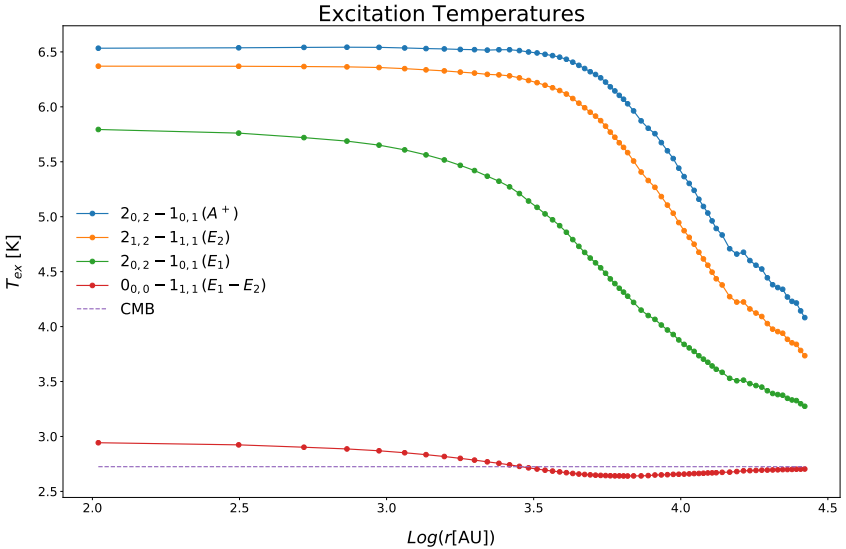

L183 & L1544

- Deeper analysis – extending molecular sample
- L1544 well studied prestellar core in Taurus
  - Several molecular studies in literature
  - Recent high-sensitivity single-pointing observations from ASAI (now publicly available)
- Literature (or in preparation) data where available
- Otherwise ASAI data – same analysis method as for L183

L183 at 3mm

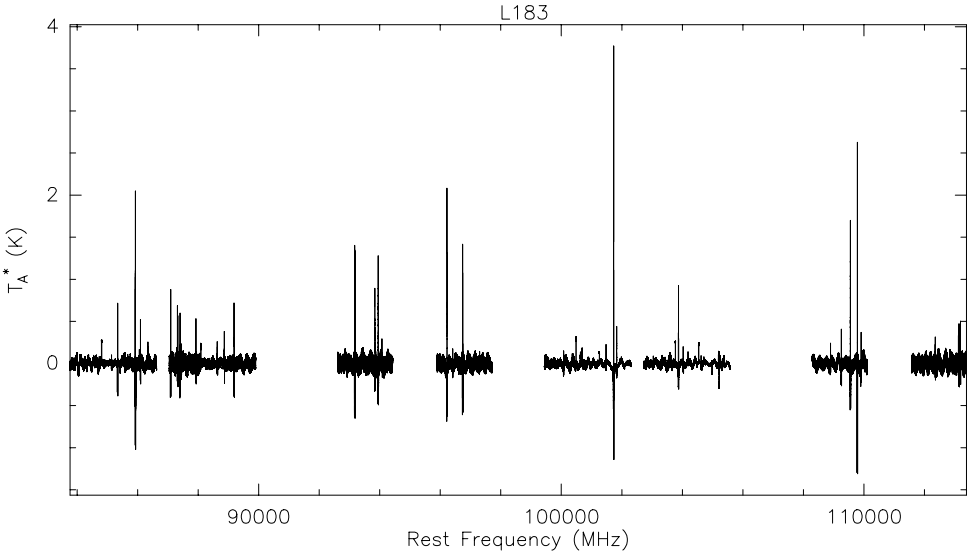

Results – I

- First Case: ≤ 2 transitions detected in L183 and no literature data for L1544.

Species	L183		L1544	
	$T_{ex} = 5\,K$	$T_{ex} = 10\,K$	$T_{ex} = 5\,K$	$T_{ex} = 10\,K$
$^{13}C^{18}O$	$(3.9\pm0.6) \times 10^{13}$	$(3.3\pm0.5) \times 10^{13}$	$(3.6\pm0.6) \times 10^{13}$	$(3.0\pm0.5) \times 10^{13}$
DC_3N	$(8.2\pm1.3) \times 10^{11}$	$(1.3\pm0.2) \times 10^{11}$	$(7.4\pm1.1) \times 10^{12}$	$(1.2\pm0.2) \times 10^{12}$
DNCO	$(1.2\pm0.2) \times 10^{12}$	$(4.9\pm0.8) \times 10^{11}$	$(2.6\pm0.4) \times 10^{12}$	$(1.0\pm0.2) \times 10^{12}$
$H^{15}NC$	$(3.8\pm0.6) \times 10^{11}$	$(3.4\pm0.5) \times 10^{11}$	$(7.5\pm1.1) \times 10^{11}$	$(6.8\pm1.0) \times 10^{11}$
$HC^{18}O^+$	$(5.7\pm0.9) \times 10^{10}$	$(5.2\pm0.8) \times 10^{10}$	$(1.3\pm0.2) \times 10^{11}$	$(1.2\pm0.2) \times 10^{11}$
$HN^{13}C$	$(1.4\pm0.2) \times 10^{12}$	$(1.3\pm0.2) \times 10^{12}$	$(2.5\pm0.4) \times 10^{12}$	$(2.3\pm0.4) \times 10^{12}$

Results – II

- Second Case: ≤ 2 transitions detected in L183 and literature data for L1544.

Species	L183		L1544	
	$T_{ex} = 5\,K$	$T_{ex} = 10\,K$	T_{ex} (K)	N_{obs} (cm^{-2})
c-C_3H_2	$(3.5\pm0.6)\times10^{12}$	$(1.4\pm0.2)\times10^{12}$	6	$(3.7\pm0.1)\times10^{13}$
c-$H^{13}CCCH$	$(1.9\pm0.3)\times10^{11}$	$(2.0\pm0.3)\times10^{11}$	6	$(9.6\pm0.4)\times10^{11}$
$C^{34}S$	$(7.8\pm1.2)\times10^{11}$	$(5.7\pm0.9)\times10^{11}$	10	$(7.8–8.3)\times10^{11}$
C_3O	$(7.6\pm1.2)\times10^{11}$	$(1.4\pm0.2)\times10^{11}$	10	2.0×10^{11}
HCS^+	$(1.8\pm0.3)\times10^{11}$	$(1.4\pm0.2)\times10^{11}$	10	$(6.2–6.5)\times10^{11}$
HDCS	$(8.1\pm1.2)\times10^{11}$	$(6.8\pm1.0)\times10^{11}$	6.8±0.6	$(1.6\pm0.8)\times10^{12}$
$HOCO^+$	$(4.4\pm0.7)\times10^{11}$	$(2.4\pm0.4)\times10^{11}$	8.5	1.9×10^{11}
NS^+	$(1.2\pm0.3)\times10^{10}$	$(8.4\pm2.1)\times10^{09}$	12	2.3×10^{10}
$S^{18}O$	$(1.2\pm0.2)\times10^{12}$	$(8.5\pm1.3)\times10^{11}$	6–8	$(3.0–3.2)\times10^{11}$
SO_2	$(3.5\pm0.5)\times10^{12}$	$(3.4\pm0.5)\times10^{12}$	12±1	$(2.0–3.5)\times10^{12}$
CH_3CCH	$(3.4\pm0.6)\times10^{12}$	$(1.8\pm0.3)\times10^{12}$	11±2	2.0×10^{13}
D_2CS	$(5.1\pm0.8)\times10^{11}$	$(4.2\pm0.6)\times10^{11}$	9.6±1.5	$(1.1\pm0.7)\times10^{12}$
$H_2C^{34}S$	$(1.8\pm0.4)\times10^{11}$	$(1.9\pm0.4)\times10^{11}$	14.1±2.0	$(3.5\pm0.7)\times10^{11}$
HNCO	$(5.8\pm0.9)\times10^{12}$	$(3.2\pm0.5)\times10^{12}$	10	$(4.0\pm1.0)\times10^{12}$
HOCN	$(7.9\pm1.4)\times10^{10}$	$(4.5\pm0.8)\times10^{10}$	10	$(4.0\pm2.0)\times10^{10}$
SO	$(6.0\pm1.0)\times10^{14}$	$(4.3\pm0.7)\times10^{14}$	9.7±1.8	$(5.2\pm0.8)\times10^{12}$
HC_3N	$(7.3\pm1.1)\times10^{12}$	$(6.1\pm0.9)\times10^{11}$	7.2±0.2	$(8.0\pm0.4)\times10^{13}$
l-C_3H_2	$(1.1\pm0.3)\times10^{11}$	$(4.1\pm1.0)\times10^{10}$	4	1.1×10^{12}

Results – III

- Third Case: 2 transitions detected in L183.
  MCMC analysis for L183 and literature data for L1544.

Species	L183		L1544	
	T_{ex} (K)	N_{obs} (cm^{-2})	T_{ex} (K)	N_{obs} (cm^{-2})
CH_3CHO	5.5±0.4	$(3.1\pm0.6)\times10^{12}$	17±1	5.0×10^{11}
t-HCOOH	8.1±0.8	$(1.4\pm0.3)\times10^{12}$	10	5.0×10^{11}
CH_3OCHO	14.9±2.0	$(1.0\pm0.1)\times10^{12}$	5.1±2.3	$(4.4\pm4.0)\times10^{12}$
H_2CCO	21.3±1.6	$(1.1\pm0.1)\times10^{12}$	27±1	5.0×10^{12}
CH_2DOH	6.8±0.5	$(1.9\pm0.2)\times10^{12}$	5–8	$(2.4\pm0.9)\times10^{12}$
OCS	11.0±1.2	$(7.4\pm1.0)\times10^{12}$	5.6±0.2	$(6.5\pm0.9)\times10^{12}$
H_2CS	12.3±0.7	$(1.7\pm0.1)\times10^{12}$	12.3±0.7	$(7.3\pm1.0)\times10^{12}$
c-C_3HD	6.5±0.8	$(6.1\pm0.7)\times10^{11}$	6	$(6.2\pm0.3)\times10^{12}$
C_4H	5.1±0.1	$(4.2\pm0.4)\times10^{13}$	10	$(1.8\pm0.6)\times10^{14}$
CCH	11.9±6.6	$(3.8\pm0.6)\times10^{13}$	4.3	$(2.4\pm0.8)\times10^{14}$
$C^{17}O$	11.5±0.8	$(5.1\pm0.1)\times10^{14}$	10	6.6×10^{14}
N_2H^+	4.6±0.1	$(1.2\pm0.2)\times10^{13}$	5.0±0.2	$(1.8\pm0.2)\times10^{13}$
NH_2D	5.6±0.1	$(2.3\pm0.1)\times10^{14}$	10	$(2.6\pm0.1)\times10^{13}$
$H^{13}CN$	3.0±0.1	$(9.4\pm0.5)\times10^{11}$	3.4±0.1	$(1.3\pm0.1)\times10^{12}$
CH_3OH	–	$(4.9\pm0.7)\times10^{13}$	–	$(2.7\pm0.6)\times10^{13}$

Column Density ratio

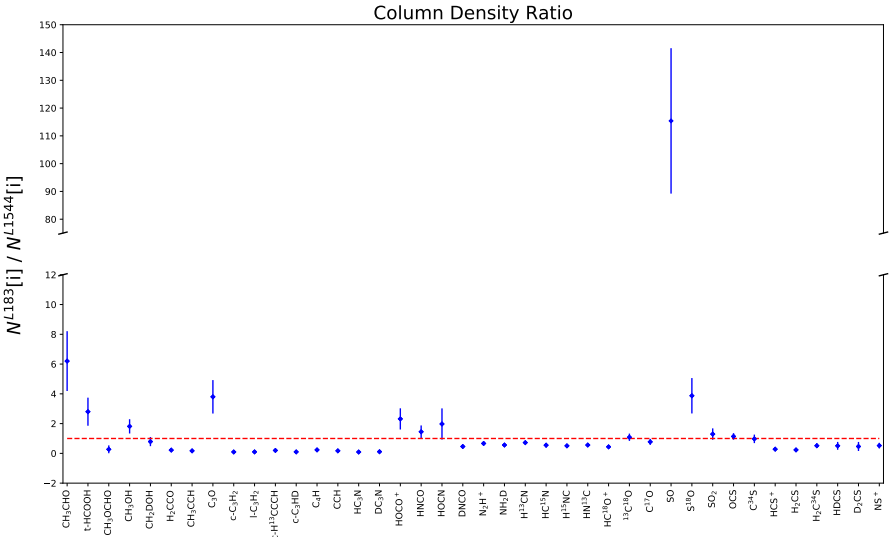

Column Density ratio

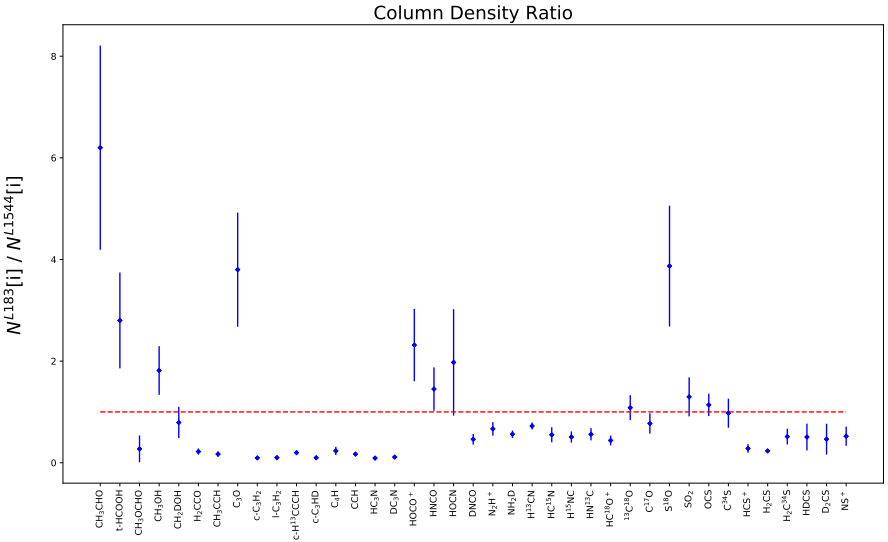

L183 and Chemical Model

- Molecular abundances compared to chemical model by Vasyunin+ (2017)
  - Advanced gas-grain astrochemical model
  - Multilayer approach to the ice-surface chemistry
  - Reactive desorption based on recent experiments
- In 2017 only iCOMs in L1544 considered
- Radial distribution of density and temperature from physical model

- Herschel beam does not resolve denser part of the core
- For the inner 3000 AU distributions combined with L1544 model density profile (Keto & Caselli 2010)

L183 and Chemical Model

- Molecular abundances compared to chemical model by Vasyunin+ (2017)
  - Advanced gas-grain astrochemical model
  - Multilayer approach to the ice-surface chemistry
  - Reactive desorption based on recent experiments
- In 2017 only iCOMs in L1544 considered
- Radial distribution of density and temperature from physical model

- Herschel beam does not resolve denser part of the core
- For the inner 3000 AU distributions combined with L1544 model density profile (Keto & Caselli 2010)

Evolution of the Chemical Model

- Larger molecular set $\rightarrow$ more challenging
- Model 2: modified initial chemical composition
  - from Diffuse Cloud (A_v =2, $n = 10^2\,cm^{-3}$) to Dark cloud (A_v =10, $n = 10^4\,cm^{-3}$)
- $\rightarrow$ no improvement.
- Model 3: Updated reaction rates, added new chemical reactions.

L183: observations VS chemical models

Species	Column Density (cm^{-2})			
	Observed	Model 1	Model 2	Model 3
SO	6.0×10^{14}	3.2×10^{14}	5.4×10^{14}	3.7×10^{14}
OCS	7.4×10^{12}	1.9×10^{12}	$\mathbf{1.5 \times 10^{11}}$	3.2×10^{12}
H_2CS	1.7×10^{12}	1.3×10^{13}	1.4×10^{13}	1.3×10^{13}
SO_2	3.5×10^{12}	$\mathbf{1.6 \times 10^{14}}$	$\mathbf{9.5 \times 10^{14}}$	$\mathbf{2.2 \times 10^{14}}$
CS	7.8×10^{12}	1.8×10^{13}	2.6×10^{12}	2.5×10^{13}
HCS^+	1.8×10^{11}	2.9×10^{10}	2.3×10^{10}	2.9×10^{10}
CH_3OCHO	1.0×10^{12}	$\mathbf{5.5 \times 10^{10}}$	$\mathbf{1.8 \times 10^{11}}$	1.2×10^{11}
HCOOH	1.4×10^{12}	9.1×10^{12}	2.0×10^{12}	8.9×10^{12}
CH_3CHO	3.1×10^{12}	3.6×10^{13}	9.9×10^{11}	1.5×10^{12}
CH_3CCH	3.4×10^{12}	1.1×10^{13}	1.1×10^{12}	1.5×10^{13}
CH_3OH	4.9×10^{13}	2.2×10^{14}	5.2×10^{13}	3.5×10^{14}
H_2CCO	1.1×10^{12}	$\mathbf{2.7 \times 10^{13}}$	5.8×10^{11}	7.4×10^{12}
N_2H^+	1.2×10^{13}	3.8×10^{12}	5.9×10^{12}	2.5×10^{12}
C_2H	6.3×10^{13}	5.1×10^{13}	$\mathbf{3.7 \times 10^{12}}$	4.9×10^{13}
C_4H	4.2×10^{13}	4.2×10^{13}	1.1×10^{13}	4.5×10^{13}
HNCO	5.8×10^{12}	8.0×10^{11}	2.1×10^{12}	8.5×10^{11}
HC_3N	7.3×10^{12}	4.9×10^{12}	$\mathbf{1.0 \times 10^{10}}$	4.1×10^{12}
HCO^+	2.9×10^{13}	1.7×10^{13}	8.8×10^{12}	1.5×10^{13}
$HOCO^+$	4.4×10^{11}	9.9×10^{10}	3.0×10^{11}	7.1×10^{10}
CO	8.5×10^{17}	5.6×10^{17}	$\mathbf{7.1 \times 10^{16}}$	6.7×10^{17}
HCN	6.0×10^{13}	5.4×10^{13}	6.2×10^{12}	6.2×10^{13}

Conclusions

- More than 100 emission features from 46 molecular species
- First detection of NS^+, Methyl Formate, and D-Methanol in L183
- Column densities compared to those found in the dust peak of L1544

- C/O differentiation of the two sources:
  - L183 is richer in O-bearing species
  - L183 core more embedded than L1544

H_2 distribution: L183 & L1544

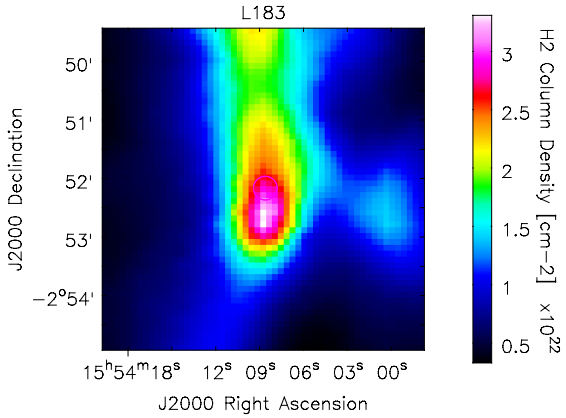

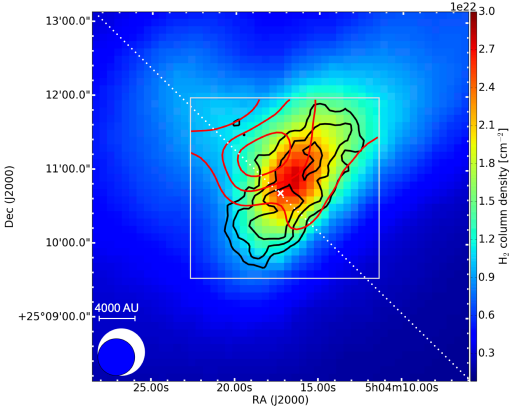

Spezzano+, 2016

Conclusions

- More than 100 emission features from 46 molecular species
- First detection of Methyl Formate and D-Methanol in L183
- Column densities compared to those found in the dust peak of L1544
- C/O differentiation of the two sources:
  - L183 is richer in O-bearing species
  - L183 core more embedded than L1544
  - Screen of the core from the ISRF
  - $\Rightarrow$ allowing most of C $\rightarrow$ CO and little for C-chains
- *Environmental conditions (more than time evolution) translate into chemical differentiation*
- SO_2 model issue:
  - $SO + OH \rightarrow SO_2 + H$
  - OH might be overestimated in the model, although consistent with previous estimations
  - Uncertain rate coefficient at low temperatures (measured only $T \geq 300\,K$)

Conclusions

- More than 100 emission features from 46 molecular species
- First detection of Methyl Formate and D-Methanol in L183
- Column densities compared to those found in the dust peak of L1544
- C/O differentiation of the two sources:
  - L183 is richer in O-bearing species
  - L183 core more embedded than L1544
  - Screen of the core from the ISRF
  - $\Rightarrow$ allowing most of C $\rightarrow$ CO and little for C-chains
- *Environmental conditions (more than time evolution) translate into chemical differentiation*
- SO_2 model issue:
  - $SO + OH \rightarrow SO_2 + H$
  - OH might be overestimated in the model, although consistent with previous estimations
  - Uncertain rate coefficient at low temperatures (measured only $T \geq 300\,K$)

Next

- Extend new chemical model to L1544
- Follow-up mapping of L183 already performed
  - Extend L183 VS L1544 comparison
  - Methanol and D-Methanol
  - Chemical differentiation
  - Environmental conditions

- L. Bizzocchi, P. Caselli, J. Harju, A. Vasyunin, C. Vastel, B. Lefloch, R. Bachiller

---

Post-Doctoral Position @ CAS on ION TRAP


MPE

Methanol non-LTE analysis

- Refined analysis using RT code MOLLIE

Keto & Rybicki, ApJ 2010

- Spherically symmetric model for density and temperature
- Based on Herschel/SPIRE maps at 250, 350, and 500 μm
- Gas and Dust temperature assumed equal (valid for $n \gtrsim 10^5 cm^{-3}$)
- 3-D models of n and T distributions averaged within spherical shells around the density maximum

L183 Physical Model

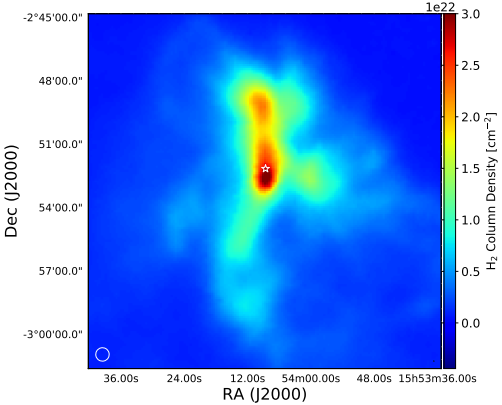

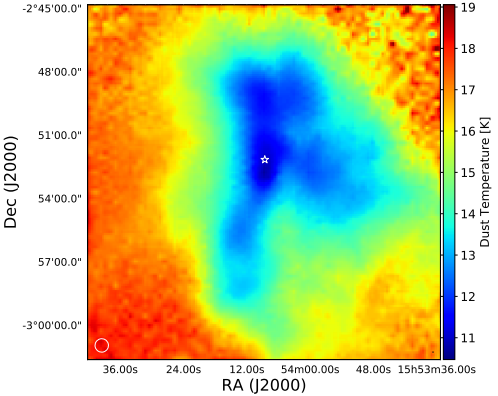

Methanol non-LTE analysis – 2

- De-excitation rates for $p-H_2/A-CH_3OH$ and $p-H_2/E-CH_3OH$ for the statistical equilibrium calculations

Rabli & Flower, MNRAS 2010

  - $o-H_2/p-H_2$ very low in pre-stellar cores
- Input: CH_3OH abundance converted into a radial abundance profile
- Output: data cube w/ spectral distribution of the emerging radiation field
  - convolution with the telescope beam
  - extract central pixel and comparing with observations
  - χ^2-fit optimization observed VS modelled spectra

Methanol non-LTE analysis – 3

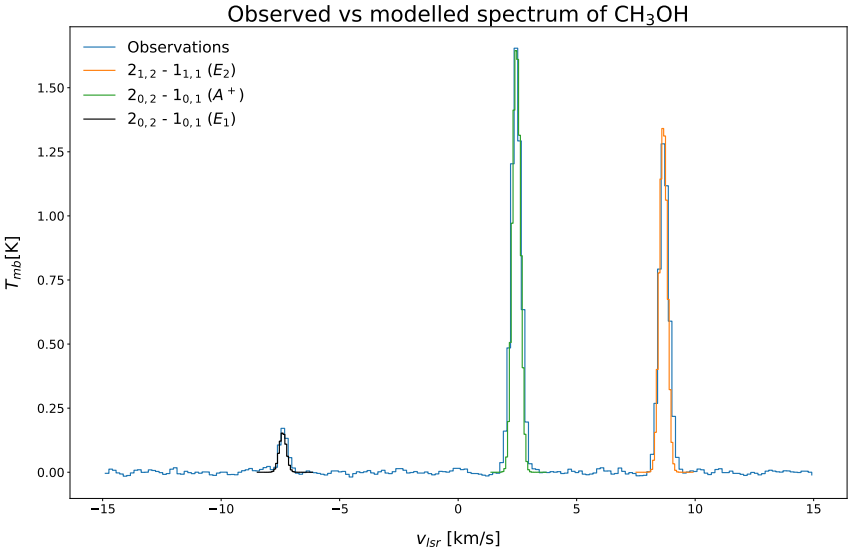

Collisional artefacts

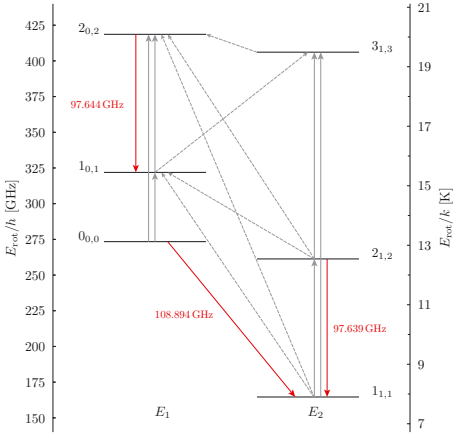

Fig. 8. Rotational energy plot for the lowest levels of *E*-CH_3OH. Active collisional channels are indicated by the upward grey arrows, with solid lines marking "strong" collisional transitions (upward rate $>10^{-11}$ cm^3 s^{-1} at 10 K, Rabli & Flower 2010a). Red solid arrows indicate the *observed* radiative transitions.

- Collisional transitions connecting $0_{0,0}$ to $1_{1,1}$ and $2_{1,2}$ have rate coefficients **set** to zero
- Artefact of the coupled state approximation
- Using 1/4 of $2_{1,2} - 1_{1,1}$ satisfactory modelling the $0_{0,0} - 1_{1,1}(E_1 - E_2)$ transition w/o altering the others

Density distribution